

## Electronic Supplementary Information (ESI)

### *Raspberry-like small multicore gold nanostructures for efficient photothermal conversion in the first and second near-infrared windows*

Anouchka Plan Sangnier,<sup>†,a,b</sup> Romain Aufaure,<sup>†,a</sup> Soshan Cheong,<sup>c</sup> Laurence Motte,<sup>a</sup> Bruno Palpant,<sup>d</sup> Richard D. Tilley,<sup>c</sup> Erwann Guenin,<sup>\*,e</sup> Claire Wilhelm,<sup>\*,b</sup> Yoann Lalatonne<sup>\*,a,f</sup>

a. Inserm U1148, LVTS, Université Paris 13, Sorbonne Paris Cité, Bobigny, France.

b. Laboratoire Matière et Systèmes Complexes, UMR 7057, CNRS and University Paris Diderot, Paris, France

c. School of Chemistry and Marck Wainwright Analytical Centre, The University of New South Wales, Australia

d. Laboratoire de Photonique Quantique et Moléculaire, CentraleSupélec, Ecole Normale Supérieure Paris-Saclay, Université Paris Saclay, CNRS UMR 8537, 3 rue Joliot Curie, F-91190 Gif-sur-Yvette, France

e. Sorbonne Universités, Université de Technologie de Compiègne, Integrated Transformations of Renewable Matter Laboratory (EA TIMR 4297 UTC-ESCOM), Compiègne, France

f. Service de Médecine Nucléaire, Hôpital Avicenne Assistance Publique-Hôpitaux de Paris, Bobigny, France.

### Materials and methods

#### 1. HMBPene synthesis

593 mg (5 mmol) of 4-pentenoyl chloride ( $\text{ClCO}(\text{CH}_2)_2\text{CHCH}_2$ , 98%, Sigma-Aldrich, St Louis, MO) were frozen in a roundbottom flask of 25 ml with liquid nitrogen, then 5 ml of tris-(trimethylsilylphosphite) ( $\text{P}(\text{OSiMe}_3)_3$ , 92%, Acros Organics) were added. A white slurry was obtained and stirred overnight. Unreacted material was evaporated under vacuum at 70 °C (0.1 Torr) for 20 minutes and hydrolyzed 4 h in 20 ml of MeOH. The solvent was removed under reduced pressure, and the remaining yellow oil was crystallized at pH 2.3 in a MeOH–H<sub>2</sub>O 9:1 system. The white solid was filtered on Büchner and the yielding was equal to 70 %.<sup>1</sup>

#### 2. Au@HMBPene NPs synthesis

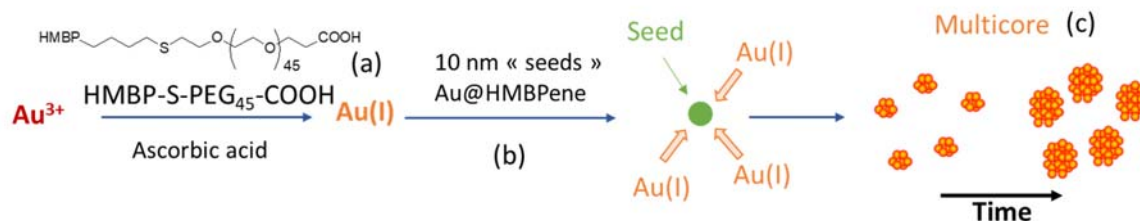
Two solutions are prepared. Solution A consists in 0.1 mmol of chloroauric acid ( $\text{HAuCl}_4 \cdot 3\text{H}_2\text{O}$ , Sigma Aldrich, 99.9 % purity) in 5 ml of ultrapure water. Solution B consists in 0.2 mmol of HMBPene in ultrapure water at pH adjusted to 9.2 with NaOH. 2 ml of solution A are added in a round-bottom flask containing 34 ml of ultrapure water. The mixture is heated under stirring with an oil bath until ebullition. Then 4 ml of B are quickly added. Solution quickly becomes pink then red and the reaction is considered completed after 10 minutes. Nanoparticles are washed 3 times with Amicon® Ultra centrifugal filters (30 kDa).<sup>1</sup>

#### 3. HMBP-S-PEG<sub>45</sub>-COOH synthesis A

All solvents are degassed prior use by bubbling argon for 10 minutes. Three solutions are prepared. Solution A: 0.25 mmol of Poly(ethylene glycol) 2-mercaptoethyl ether acetic acid, Mn 2,100, (Sigma-Aldrich) are dissolved in 3 ml of dimethylformamide (DMF). Solution B: 0.159 mmol of HMBPene are dissolved in 3 ml of ultrapure water. Solution C consists in a small amount of 1-hydroxycyclohexylphenyl ketone (Alfa Aesar, ≥ 98.0%) dissolved in DMF. Solutions A and B were mixed in a 20-ml glass vial then C was added and the tube is sealed. Solution is let under magnetic stirring and UV light (360 nm) for 5 hours. 8 ml of water are then added to the mixture and the resulting solution is washed 3 times with 10 ml of dichloromethane and 3 times 10 ml of diethyl ether. The aqueous solution is then lyophilized and a white powder is obtained. This protocol yields from 80 to 90 % of pure product (products are obtained as monosodium salts).<sup>2</sup>

#### 4. Nanoraspberries synthesis

Four solutions are prepared. Solution A consists in 2.5 ml of 2.1 mM HMBP-S-PEG<sub>45</sub>-COOH in water at pH=4. Solution B consists in 20 mM of chloroauric acid (HAuCl<sub>4</sub>, 3H<sub>2</sub>O, Sigma Aldrich, 99.9 % purity). Solution C is ascorbic acid (Sigma-Aldrich, ≥ 99,0%) at 100 mM. Solution D consists in Au@HMBPene NPs at 0.65 mM. 63 μl of solution B are added to solution 1 and manually homogenized. The mixture becomes light yellow. Then 19 μl of solution C are added and the solution becomes colorless. Quickly after, 60 μl of solution D is added, homogenized then let without agitation. Nanoparticles are washed twice with Amicon® Ultra centrifugal filters (100 kDa). The yield of the nanoraspberry synthesis was measured by ICP-AES, with a value found to be equal to 85%.



Scheme S1. Chemistry strategy for nanoraspberries design

### 5. Gold nanorods

Gold nanorods presenting a peak absorbance at 680 nm and gold nanorods presenting a peak absorbance at 810 nm were purchased from nanoComposix. Typical UV curves are provided in Fig. S5.

### 6. ICP analysis

The concentrations of gold samples were measured by elemental analysis using an ICP-AES spectrometer (iCAP6200 duo THERMOFISHER). Samples were digested in a HNO<sub>3</sub> and HCl solution (5 ml), evaporated, then solubilized in a 1% HCl solution for the Au analysis and 2% HNO<sub>3</sub> for P and S analysis. Calibration curves were performed between 10 and 1000 ppb. Calibration standards and quality controls were provided by SCPSCIENCE and ChemLab. For cellular samples analysis, cells were fixed with 2% glutaraldehyde in 0.1 M cacodylate buffer.

### 7. Absorbance analysis

UV-vis spectra were recorded on a Varian Cary 50 Scan UV-vis spectrophotometer. For the in-situ growth, the synthesis was directly performed in a spectrophotometry cuvette.

### 8. HRTEM and STEM-EDS analysis

10 μl of diluted nanoraspberries suspension were deposited onto 200 mesh copper grids covered by a carbon film. Scanning/transmission electron microscopy (S/TEM) imaging and energy-dispersive X-ray spectroscopy (EDS) elemental analysis were performed on a JEOL JEM-F200 (cold-field-emission gun, 200 kV) equipped with an annular dark-field detector and a JEOL windowless 100 mm<sup>2</sup> silicon drift X-ray detector. EDS data processing and analysis were carried out using the Thermo Scientific Pathfinder X-ray Microanalysis Software. Size distribution was determined using Fiji software<sup>3</sup> after thresholding the images and measuring the particles area.

### 9. Infrared spectroscopy

The grafting of the molecules at the surface of the particles was confirmed with Fourier Transformed Infrared Spectroscopy (FTIR) analysis. Spectra were recorded on a Thermo Scientific Nicolet 680 FTIR. Sample were analyzed as KBr pellets. Each analysis was composed of 32 acquisitions with a resolution of 1.929 cm<sup>-1</sup>.

### 10. Hydrodynamic diameter and zeta potential

Hydrodynamic diameter and zeta potential were measured with a Zetasizer Nano-ZS (Malvern, U.K.). The general purpose analysis model was used to convert the dynamic light scattering (DLS) data into a

size distribution (in volume) and the Schmoluchowski model to calculate the zeta potential. Stability of nanoraspberries in physiological medium was assessed by measuring the hydrodynamic diameter (volume) in DLS over two days in Hank's Balanced Salt Solution (HBSS), PBS and RPMI supplemented with 10% fetal bovine serum of 0.1 mM nanoparticles.

### 11. Photothermia in aqueous dispersion

Photothermal measurements were made in 1.5 ml Eppendorf tubes containing 100  $\mu$ l of aqueous samples. Concentrations were adjusted between [Au] = 0.125 mM to [Au] = 2 mM. The samples were illuminated with 680, 808 and 1064 nm lasers (Laser Components S.A.S France), always positioned 4.5 cm above (see Fig. S4 for the set-up), and adjusted to deliver a power density at 0.3 W/cm<sup>2</sup>. Temperature was recorded with an infrared thermal imaging camera (FLIR SC7000) in real time and processed with the ALTAIR software. The heating was quantified with the plateau temperature (measured after 5 min of exposure), directly provided by the thermal IR measurements, and with the specific absorption rate (SAR), meaning the power dissipated per unit mass of gold (W.g<sup>-1</sup>). SAR was calculated using the following equation:

$$SAR = \frac{C_w \cdot m_s}{m_{Au}} \cdot \frac{dT}{dt}$$

with  $C_w$  is the specific heat capacity of the sample assimilated to the one of water ( $C_w = 4.185$  J/g/K),  $m_{Au}$  is the total mass of gold in the sample (g),  $m_s$  is the total mass of the sample (g) and  $dT/dt$  is the slope of the temperature increase over the first 30 seconds when laser is turned on, as illustrated in supplementary Fig. S4c.

### 12. Light-to-heat conversion efficiency parameter

- Light-to-heat conversion coefficient parameter

Calculation was adapted from Jiang et al.<sup>4</sup> The light-to-heat conversion efficiency parameter ( $\eta$ ) was calculated as follows:  $\eta = \frac{\Delta T \cdot m_s \cdot C_w \cdot B}{P_0 - \frac{P_0}{10^A}}$  (2)

With  $\Delta T$  the temperature increase ( $^{\circ}$ C),  $m_s$  the total mass of the sample,  $C_w$  the specific heat capacity of water,  $C_w = 4.185$  J/g/K,  $P_0$  the incident laser power,  $A$  the absorbance of the sample and  $B$  the constant rate of heat dissipation from the solution to the external environment.  $A$  is calculated thanks to the Beer Lambert equation:  $A = \epsilon \cdot l \cdot c$ , with  $\epsilon$  the absorption coefficient detailed in Table S2,  $l$  the sample's length equal to 0.7 cm for the 100  $\mu$ l samples, and  $C$  the sample's concentration.  $B$  is measured during heat relaxation as:  $e^{-Bt} = \frac{T(t) - T_0}{T_m - T_0}$  (3)

With  $T(t)$  the temperature at a time  $t$ ,  $T_0$  the initial temperature of the sample before photothermal heating and  $T_m$  the maximum temperature reached after 5 minutes exposure to laser.

$B$  was calculated for all the samples with an average value of  $0.010 \pm 0.002$  s<sup>-1</sup>.

As a consequence from (2), at high concentrations,  $10^{-A}$  becomes negligible and  $\Delta T$  is directly proportional to  $\eta$ .

Values of the conversion coefficient extracted from the literature are presented in Table S1, together with the one found here for the nanoraspberries, confirming the nanorods values found here, and showing lower values for other state-of-the-art gold nanostars or nanoshells.

GNPs shape	nanoraspberries	nanorods <sup>5</sup>	nanostars <sup>6</sup>	nanoshells <sup>5</sup>
$\eta$ (%)	65	65	35	35

Table S1. Coefficient of conversion efficiency ( $\eta$ ) for state-of-the-art gold nanoheaters within the biological window.

### - SAR dependence on Au concentration

SAR dependence to the Au concentration is explained by adapting calculation from Jiang et al.<sup>4</sup> The energy input  $Q_{in}$  by nanoparticles under laser irradiation can be defined as:

$$Q_{in} = P_0 \cdot (1 - 10^{-A}) \cdot \eta = m_{sample} \cdot C \cdot \frac{dT}{dt} \quad (4)$$

$$\text{As a consequence from (1) and (4): } SAR = \frac{P_0 \cdot (1 - 10^{-A}) \cdot \eta}{m_{Au}} \quad (5)$$

As a consequence from (5), at high concentrations,  $10^{-A}$  becomes negligible and  $SAR \approx \frac{P_0 \cdot \eta}{m_{Au}}$ .

### 13. Cell culture and multicores internalization

Human prostate cancer (PC3) cells were purchased from ATCC. They were cultured in Dulbecco's modified Eagle's medium (DMEM) supplemented with 10% fetal bovine serum (FBS) and 1% penicillin-streptomycin (PS) at 37°C with 5% CO<sub>2</sub> until they reach 90% confluence. Cells were then incubated with multicore gold nanoparticles. NPs were dispersed in RPMI-1640 medium for 17 hours at gold concentrations equal to 15 and 6.5 μM. One T75 flask was prepared per condition. Cells were then washed twice with multicore-free RPMI-1640 medium and left 2 hours in PS and FBS supplemented DMEM for a chase period.

### 14. Photothermia in cells

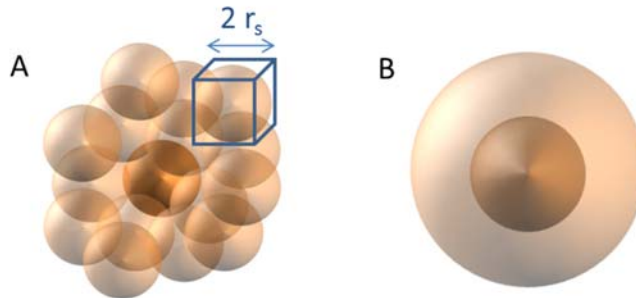
Photothermal measurements were made in 1.5 ml Eppendorf tubes. Cells were detached from the T75 flask with Trypsin-EDTA (0.05 %), phenol red (ThermoFisher Scientific). Each sample was positioned in a thermostated cuve at 37 °C and was illuminated with a 680 nm, a 808 nm and a 1064 nm laser (Laser Components S.A.S France) positioned 4.5 cm above the sample at 0.3 W.cm<sup>-2</sup> for 10 minutes. The temperature was recorded with an infrared thermal imaging camera (FLIR SC7000) in real time and was processed with ALTAIR software. Cells were then deposited in T75 flasks in DMEM medium supplemented with 1% PS and 10% FBS and let for 24 hours until cytotoxic assay.

### 15. Cytotoxicity assay

Cytotoxicity assay was performed on cells using the APC Annexin V Apoptosis Detection Kit with propidium iodide (Biolegend). 24 hours after laser treatment, cells were detached from the T75 with Trypsin-EDTA (0.05 %), phenol red (ThermoFisher Scientific), counted, washed twice in PBS and concentrated at 5×10<sup>6</sup> cells/ml in Annexin V binding buffer. APC Annexin V (5 μl) and Propidium Iodide (PI, 10 μl) were added to 100 μl of cell suspension (5×10<sup>6</sup> cells/ml) in 5 ml tubes. After 15 min of incubation, Annexin V binding buffer (400 μl) was added to each tube. Samples were analysed with a Cyan ADP 9C flow cytometer (Beckman Coulter, Imagoseine platform, Institute Jacques Monod, Paris).

### 16. Models to estimate the nanoraspberries size

The seed-mediated synthesis reported consists in the growth of Au salt precursor on a 10 nm spherical gold seed. The shell around the seed can be considered either as a set of spheres of radii  $r_s$ , each occupying a cubic volume  $V_{cube}$  (Model 1: nanoraspberry shell) or as a homogeneous growth (Model 2: compact shell).



Scheme S2. Schematic representation of (A) a network of spheres around each gold nanoparticle seed of 10 nm (Model 1) and (B) a compact shell around each seed (Model 2)''

### **Model 1: nanoraspberry shell**

The rasperry shell is considered as a compact set of spheres of radii  $r_s$  occupying a cubic volume  $V_{cube} = (2r_s)^3$  each (Scheme S2A). The total gold volume ( $V_{Rasp}$ ) is the sum of the seed volume ( $V_{seed}$ ) and the shell volume ( $V_{shell}$ ) around the 10-nm seed.

First, the 10 nm seed volume is equal to:  $V_{seed} = \frac{4}{3}\pi r_{seed}^3 = \frac{4}{3}\pi 5^3 = 523.6 \text{ nm}^3$

Then, the set of sphere volume ( $V_{shell}$ ) is:  $V_{shell} = N_{sphere} V_{cube}$ , with  $N_{sphere} = \frac{N(Au)_{shell}}{N(Au)_s}$

$N(Au)_{shell}$  is the total number of Au atoms per nanoraspberry shell and  $N(Au)_s$  is the number of Au atoms per individual shell sphere.

$N(Au)_{shell}$  is calculated by considering that each nanoraspberry is growing from one nanoparticle seed:

$$N(Au)_{shell} = \frac{[Au]}{[seeds]}$$

with  $[Au]$  the gold salt concentration and  $[seeds]$  the 10 nm nanoparticles seed concentration.

Because each crystalline lattice contains 4 Au atoms,  $N(Au)_{shell} = 4 \frac{V_{shell}}{V_{lattice}}$ , with  $V_{lattice}$  the crystalline lattice volume.

Finally, we obtain  $N(Au)_{shell} = \frac{16\pi}{3} \frac{r_s^3}{V_{lattice}}$ .

Consequently the nanoraspberry volume is:

$$V_{shell} = \frac{3[Au]V_{lattice}}{16\pi[seeds]r_s^3} V_{cube} = \frac{3[Au]V_{lattice}}{16\pi[seeds]r_s^3} (2r_s)^3 = \frac{3[Au]V_{lattice}}{2\pi[seeds]}$$

63  $\mu$ l of Au salts at  $[Au]=20$  mM were added to a 2.642 ml total volume. This took into account the 85% synthesis yield ratio determined by ICP-AES, with final concentration  $[Au] = 20 * 0.85 * (63/2642) = 0.405$  mM; 60  $\mu$ l of seeds at  $[Au]=0.65$ mM corresponds to 21.1 nM of 10 nm-seed, and were added to the 2.642 ml solution. Therefore  $[seeds] = 21.1 \times 10^{-6} * (60/2642) = 0.48 \times 10^{-6}$  mM

$V_{lattice}$  is equal to  $a^3 = 0.0679 \text{ nm}^3$ , with  $a = 0.408 \text{ nm}$ .

Therefore,  $V_{shell} = 27354 \text{ nm}^3$ , and finally  $V_{Raspb} = V_{shell} + V_{seed} = 27354 + 523.6 = 27877,6 \text{ nm}^3$

Consequently the nanoraspberry diameter is equal to  $D_{Raspb} = 2 \sqrt[3]{\frac{3 \times V_{Raspb}}{4\pi}} = 37.62 \text{ nm}$

### **Model 2: Compact shell**

The compact shell model considers a homogeneous gold shell around each seed forming the nanoparticle (Scheme S2b).

Each crystalline lattice contains 4 Au atoms:

$$N(Au)_{total} = 4 \frac{V_{nano}}{V_{lattice}}$$

$N(Au)_{total}$  is defined considering that each core-shell GNP is growing on one GNP seed:

$$N(Au)_{Total} = \frac{[Au]_{Total}}{[seeds]}$$

Consequently:  $V_{nano} = \frac{V_{lattice} \times \frac{[Au]_{total}}{[seeds]}}{4}$

with (see above model 1): [Au]salt = 0.405 mM; [Au]seed = 0.65 x (60/2642) = 0.0148 mM; [seeds] = 0.48 x 10<sup>-6</sup> mM;  $V_{lattice} = 0.0679 \text{ nm}^3$

$$V_{core-shell} = \frac{0.0679 \times \frac{(0.405+0.0148)}{0.48 \times 10^{-6}}}{4} = 14846 \text{ nm}^3$$

Consequently the corresponding core-shell diameter is equal to:

$$D_{core-shell} = 2 \sqrt[3]{\frac{3 \times V_{core-shell}}{4\pi}} = 30.49 \text{ nm}$$

### 17. Coating density calculation

Concentration of P, S and Au were determined by elemental analysis (ICP-AES). 0.09 ± 0.01 HMBP-S-PEG<sub>45</sub>-COOH molecule per Au atom were obtained by taking into account that each HMBP-S-PEG<sub>45</sub>-COOH molecule contains 2 P atoms and 1 S atom.

The number of Au atom per growth sphere is (see nanoraspberry model):

$$n(Au)_s = \frac{16\pi}{3} \frac{r_s^3}{V_{lattice}} = \frac{16\pi}{3} \frac{(3.2)^3}{0.0679} = 8086$$

We can deduce an amount of HMBP-S-PEG<sub>45</sub>-COOH molecule per growth sphere equal to: (0.09 ± 0.01)\*8086 = 728 ± 81

The surface area of a growth sphere is:

$$S_{1\ sphere} = 4\pi r_{sphere}^2 = 4 \times \pi \times (3.2 \pm 0.35)^2 = 128.7 \pm 28.1 \text{ nm}^2$$

Therefore the coating density can be estimated to a surface area of (128.7±28.1)/(728±81) nm<sup>2</sup>, that is 18 ± 6 Å<sup>2</sup>

## Supplementary figures

### 1. Nanoraspberry size control

The nanoraspberry size was modulated by varying the concentration ratio between the Au salt precursor and the Au seeds. The Au salt precursor concentration was kept constant (0.405 mM) whereas the Au seed was varied from 0.08 nM (Figure S1 a), 0,24 nM (Figure S1 b) and 0,48 nM (Figure S1c) leading to nanoraspberries sizes of 73, 51 and 37 nm, respectively. The smallest ones are the ones further exploited in the manuscript.

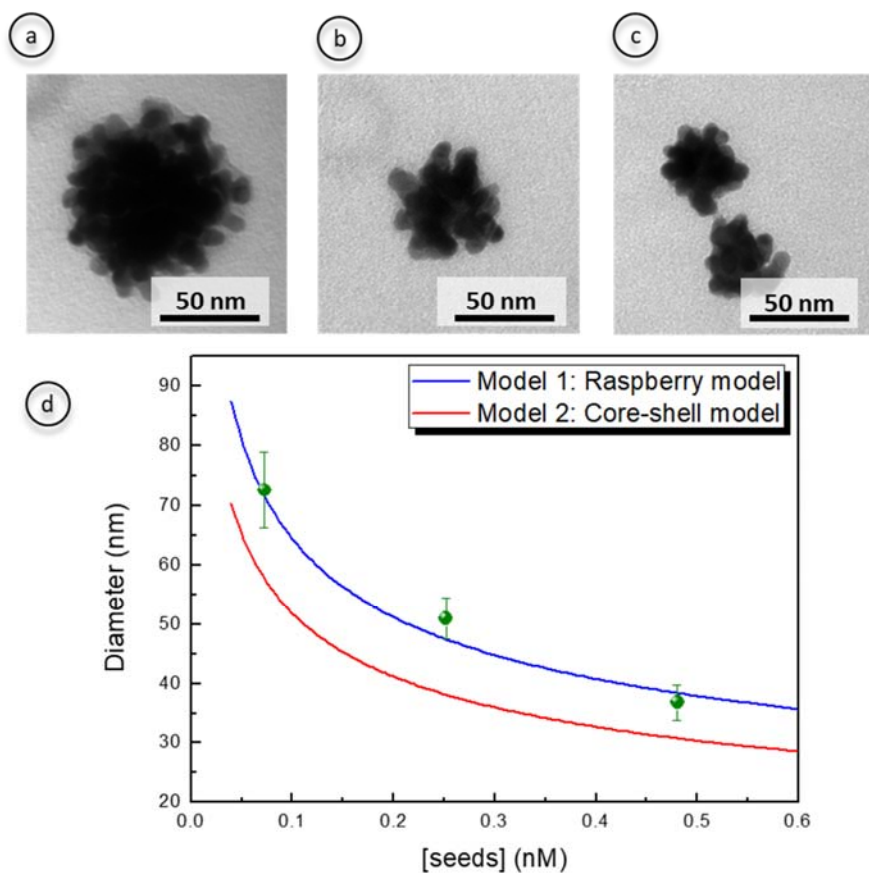


**Fig. S1:** TEM images of nanoraspberries obtained with seeds concentration at (a) 0.08; (b) 0.24 and (c) 0.48 nM of Au and (d) mean size evolution (green dots) with seeds concentration. The results obtained with the nanoraspberry model 1 (blue curve) and the core-shell model 2 (red curve) are shown on the same plot.

## 2. FFT spectra

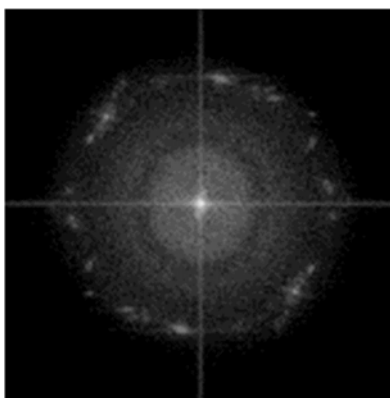


**Fig. S2:** polycrystalline structure of the nanoraspberries indicated by the FFT of Figure 1c.

### 3. Nanoraspberry surface

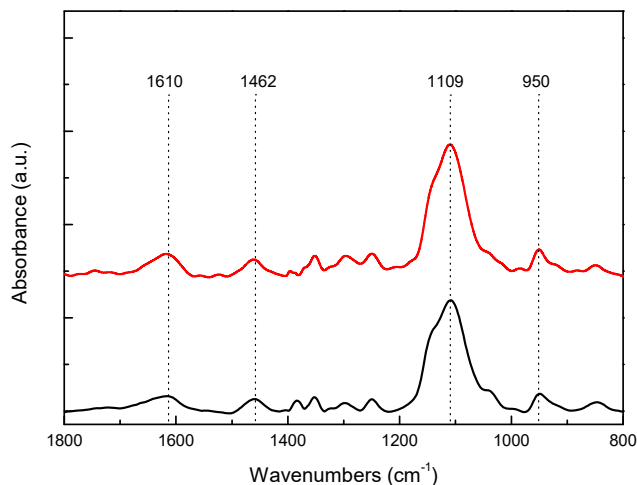


**Fig. S3.** FTIR spectra of HMBP-S-PEG<sub>45</sub>-COOH molecules (red curve) and nanoraspberries (black curve). Both spectra are similar demonstrating the presence of HMBP-S-PEG<sub>45</sub>-COOH molecules on the nanoraspberries surface. In particular, PEG chains are detected by a strong C-O vibration at 1110 cm<sup>-1</sup>. Carboxylic groups show the two characteristic bands at 1610 and 1462 cm<sup>-1</sup> due to the carboxylic vibration band and symmetric carboxylate stretches respectively, and bisphosphonates are evidenced by the P-OH vibration band at 950 cm<sup>-1</sup>.

### 4. Nanoraspberry colloidal dispersion

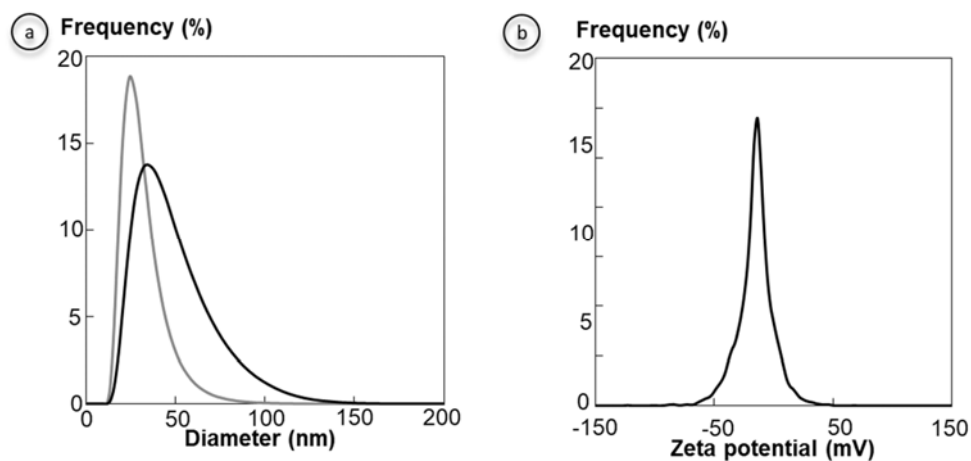


**Fig. S4.** (a) Hydrodynamic diameter distribution in volume (black curve) and in number (grey curve) (PDI = 0.218). (b) zeta potential measured in water (pH=7.4)

## 5. Photothermal experimental set up and extracted data

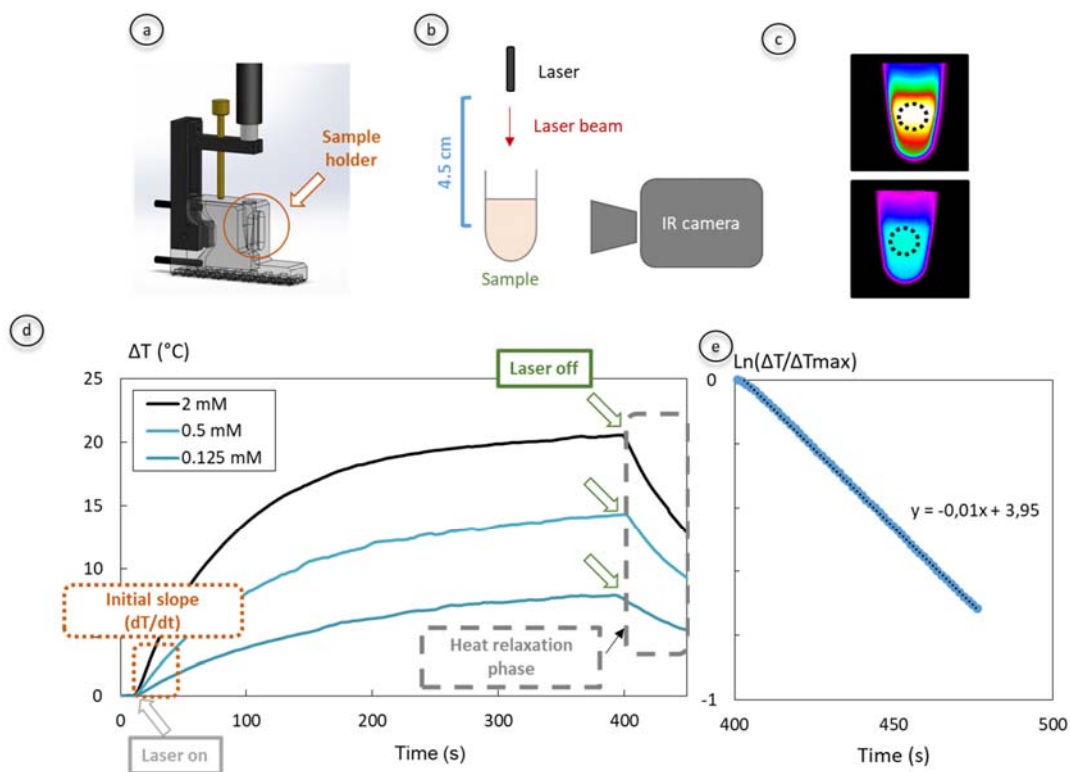


**Fig S5:** Photothermal experiment. (a) Home-made device for laser application: Laser is positioned at 4.5 cm on top of the 1.5 ml Eppendorf tube for the irradiation. Recording is made with an infrared camera. (b) Scheme illustrating the geometry of the measurement. (c) Typical IR images of irradiated tubes. The temperature is averaged within the dotted disc, with same 14 mm<sup>2</sup> area for all measurements. (d) Typical heating curves, obtained with the nanoraspberries, for different [Au] concentrations. The sample is put in the device for 1 min before starting recording, to equilibrate the temperatures of the solution and its environment. The camera then starts recording, and laser is turned on after 10 seconds and turned off after 350 seconds. The first 30 seconds of laser irradiation are used to measure the slope  $\frac{dT}{dt}$ , directly used to calculate the SAR for the given condition (see methods). When laser is turned off, the slope of the heat relaxation phase is also measured, and used to calculate the parameter B, in the light-to-heat conversion formula to retrieve the efficiency coefficient  $\eta$  (see methods). (e) Typical plot of  $\ln\left(\frac{\Delta T}{\Delta T_{max}}\right)$  during the heat relaxation phase. The slope is equal to  $-B$ .

## 6. Absorbance curves and absorption parameters

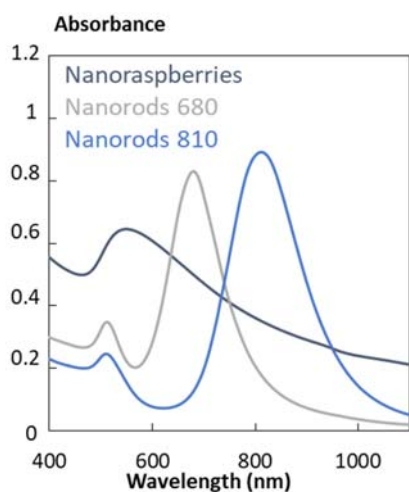


**Fig. S6.** Typical absorbance curves of nanoraspberries and nanorods at the same concentration  $[Au] = 0.12 \text{ mM}$ .

	680 nm	808 nm	1064 nm
Nanorods 680	$9445 \pm 474$	$2081 \pm 104$	$277 \pm 14$
Nanorods 810	$1402 \pm 70$	$10137 \pm 509$	$841 \pm 43$
Nanoraspberries	$5657 \pm 455$	$4000 \pm 322$	$2537 \pm 205$

**Table S2:** Values of the absorption coefficient  $\epsilon$  (in  $\text{M}^{-1} \cdot \text{cm}^{-1}$ ) calculated from the UV-Vis measurements, for the three wavelengths corresponding to the lasers used, and considering Au concentration determined by ICP-AES.

## 7. Photothermal properties of nanoraspberries and nanorods

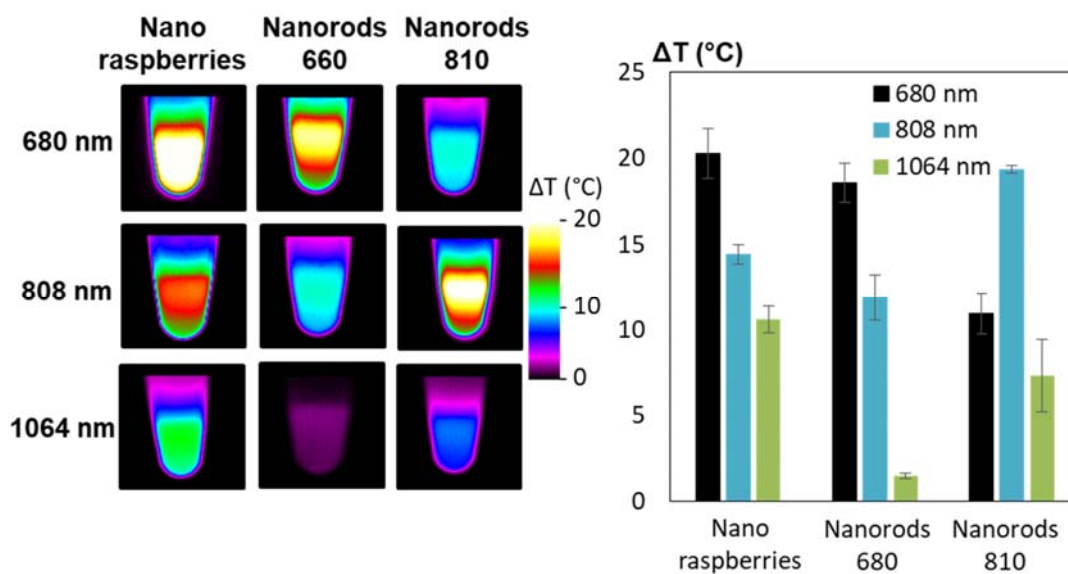


**Fig. S7.** Left: typical infrared images of nanoraspberries and nanorods at  $[Au]=0.5 \text{ mM}$ , after 5 minutes illumination at different wavelengths (680 nm, 808 nm and 1064 nm), generating photothermia (0.3

W/cm<sup>2</sup>). Right: average temperature elevation ( $\Delta T$ , in °C) for PTT at 0.3 W/cm<sup>2</sup> with lasers 680 nm, 808 nm and 1064 nm at [Au]=0.5 mM for nanoraspberries and nanorods.

### 8. SAR values of nanoraspberries and nanorods

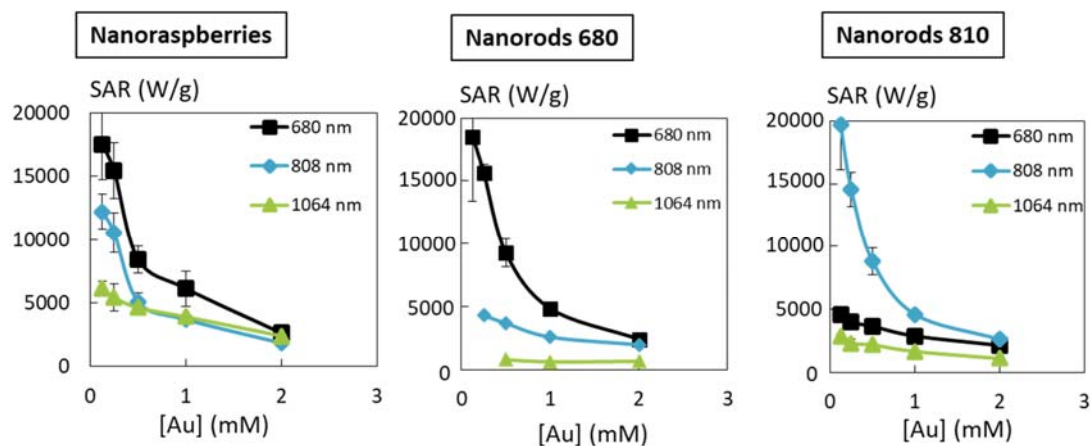


**Fig. S8.** SAR values of nanoraspberries and nanorods as a function of Au concentration after illumination (0.3 W/cm<sup>2</sup>) at different wavelengths 680 nm, 808 nm and 1064 nm.

### 9. Light-to heat conversion coefficient parameter

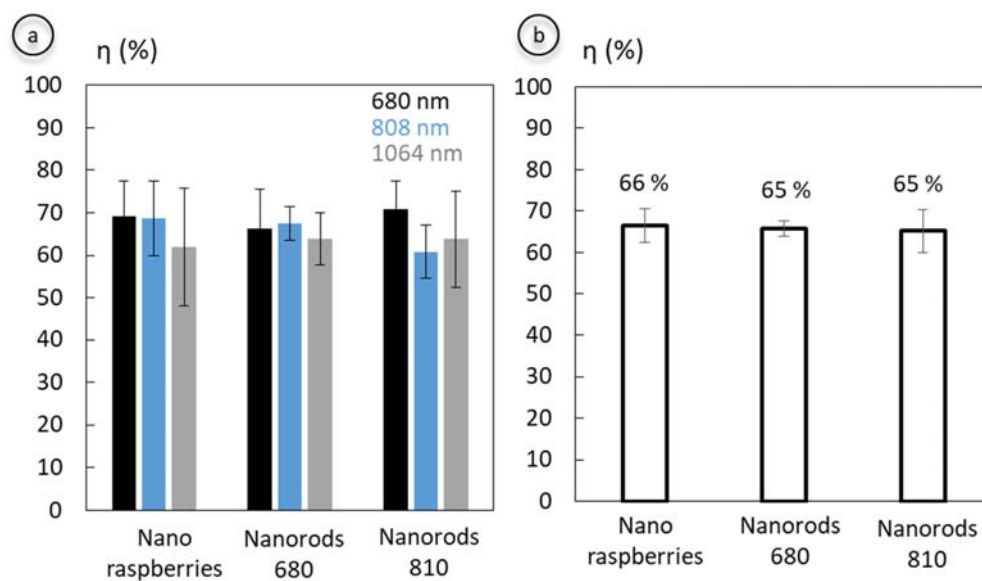


**Fig. S9:** (a). Light-to-heat conversion coefficient parameter ( $\eta$ ) calculated for each laser at 680, 808 and 1064 nm wavelengths, for nanorods and nanoraspberries. (b). Value of the light-to-heat conversion coefficient parameter ( $\eta$ ) averaged over the three lasers 680, 808 and 1064 nm, for each nanomaterial (nanorods and nanoraspberries). The error bars represent the standard deviation between all measurements (either at single wavelengths, or for all wavelengths averaged together).

10. Dependence of concentration and laser power on the temperature increase

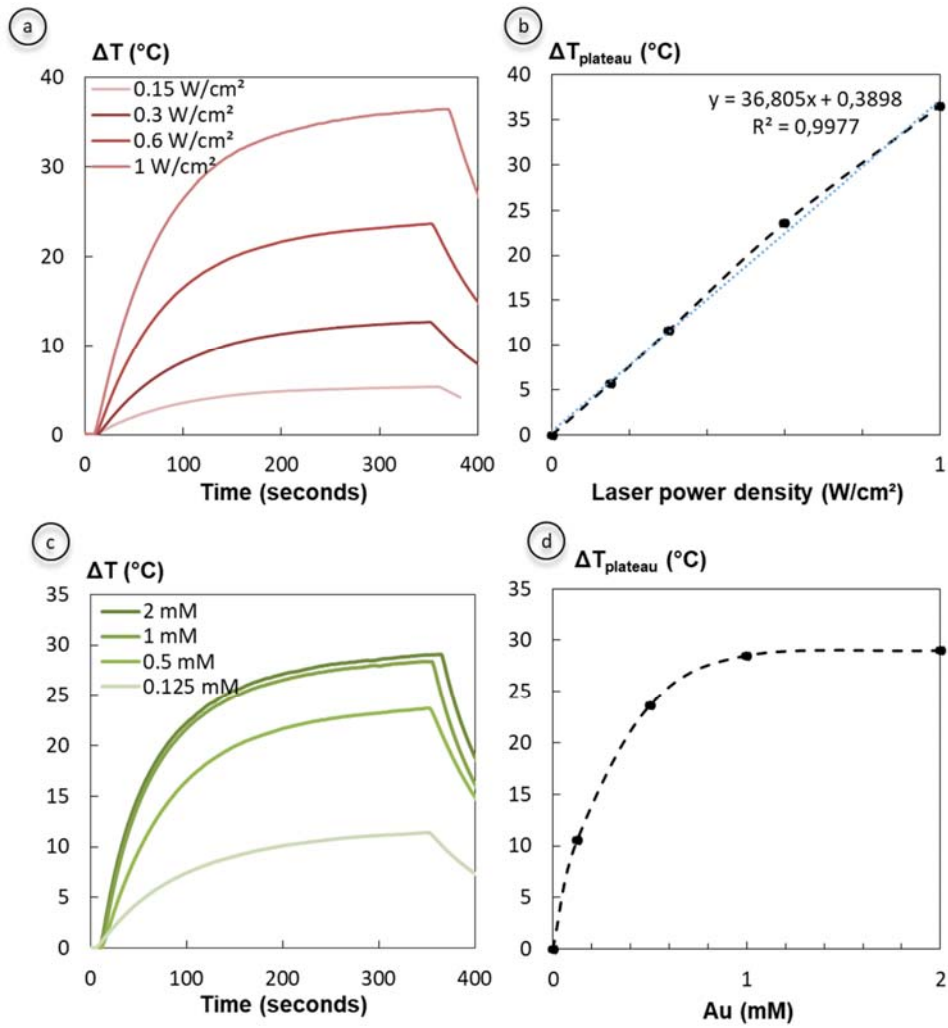
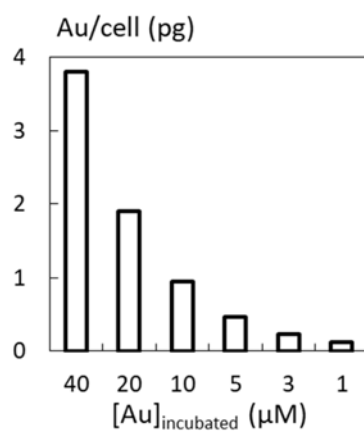


Fig. S10: (a). Typical curves  $T(t)$  for the nanoraspberries irradiated with laser 808 nm, at different power densities of 0.15, 0.3, 0.6, and 1 W/cm<sup>2</sup> at 0.5 mM. (b) Plot of the plateau temperature as a function of the laser intensity, with perfect linear dependence. (c) Typical curves  $T(t)$  for the nanoraspberries irradiated with laser 808 nm, at power density of 0.6 W/cm<sup>2</sup>, and for different [Au] concentrations, in between 0.25 and 2.0 mM. (d) Plot of the plateau temperature (for 0.6 W/cm<sup>2</sup> laser intensity) as a function of the sample concentration, which clearly shows a saturation at a temperature elevation of ~36 °C.

### 11. Cellular uptake of nanoraspberries in PC3 cells



**Fig. S11:** Uptake of nanoraspberries in PC3 prostatic cancer cells after 17 h of incubation. Mass of gold per cell was quantified by ICP-AES.

12. PC3 viability after nanoraspberries internalization and/or PTT treatment at 808 nm and 1064 nm

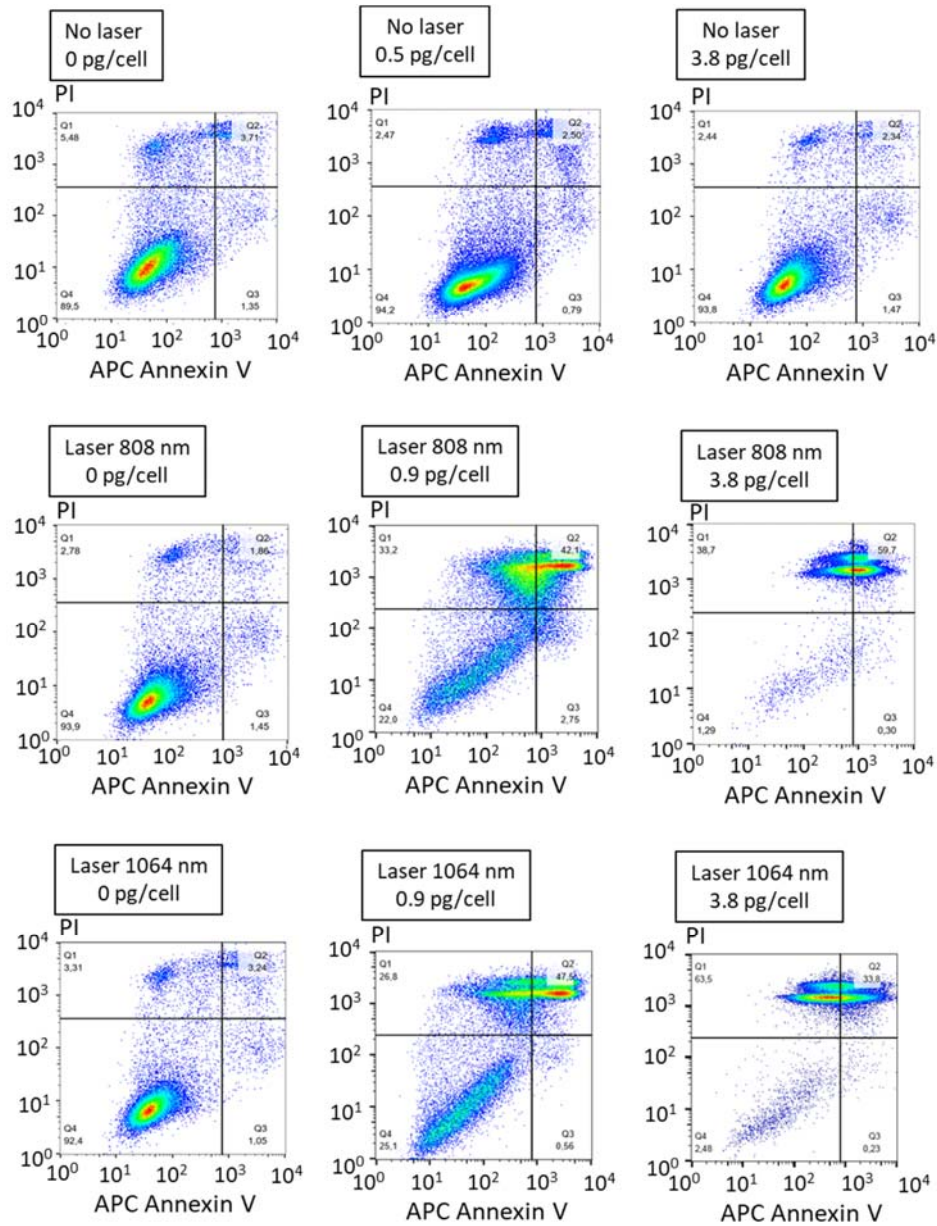


**Fig. S12.** Apoptotic and necrotic cells 24 hours post treatment quantified by flow cytometry with Annexin V and propidium iodide (PI). The different conditions correspond to cells not exposed to laser irradiation without nanoraspberries, or with 0.9 pg or 3.8 pg of nanoraspberries per cell, or for cells irradiated with laser 808 or 1064 nm (0.3 W/cm<sup>2</sup>) for the same conditions without or with nanoraspberries.

## References

1. Afaure, R.; Lalatonne, Y.; Lievre, N.; Heintz, O.; Motte, L.; Guenin, E. One pot microwave assisted synthesis of bisphosphonate alkene capped gold nanoparticles. *RSC Advances* **2014**, *4* (103), 59315-59322.
2. Afaure, R.; Buendia, R.; Motte, L.; Hardouin, J.; Lalatonne, Y.; Guenin, E. Versatile "click" synthesis of 1-hydroxy-1,1-methylenebisphosphonic acids with thioalkoxy substituents for the preparation of stable gold nanoparticles. *New Journal of Chemistry* **2017**, *41* (20), 12153-12158.
3. Schindelin, J.; Arganda-Carreras, I.; Frise, E.; Kaynig, V.; Longair, M.; Pietzsch, T.; Preibisch, S.; Rueden, C.; Saalfeld, S.; Schmid, B.; Tinevez, J.-Y.; White, D. J.; Hartenstein, V.; Eliceiri, K.; Tomancak, P.; Cardona, A. Fiji: an open-source platform for biological-image analysis. *Nature Methods* **2012**, *9*, 676.
4. Jiang, K.; Smith, D. A.; Pinchuk, A. Size-Dependent Photothermal Conversion Efficiencies of Plasmonically Heated Gold Nanoparticles. *The Journal of Physical Chemistry C* **2013**, *117* (51), 27073-27080.
5. Cole, J. R.; Mirin, N. A.; Knight, M. W.; Goodrich, G. P.; Halas, N. J. Photothermal Efficiencies of Nanoshells and Nanorods for Clinical Therapeutic Applications. *The Journal of Physical Chemistry C* **2009**, *113* (28), 12090-12094.
6. Espinosa, A.; Kolosnjaj-Tabi, J.; Abou-Hassan, A.; Plan Sangnier, A.; Curcio, A.; Silva, A. K. A.; Di Corato, R.; Neveu, S.; Pellegrino, T.; Liz-Marzán, L. M.; Wilhelm, C. Magnetic (Hyper)Thermia or Photothermia? Progressive Comparison of Iron Oxide and Gold Nanoparticles Heating in Water, in Cells, and In Vivo. *Advanced Functional Materials* **2018**, *28* (37), 1803660.